International Journal of Multiphase Flow 147 (2022) 103886

Contents lists available at ScienceDirect

International Journal of Multiphase Flow

journal homepage: www.elsevier.com/locate/ijmulflow

Repeatability in a multiphase pipe flow case study

Andreas Strand [a,*], Christian Brekken [b], Paul Roger Leinan [b], Ingelin Steinsland [c], Leif Rune Hellevik [a]

[a] Biomechanics Division, Department of Structural Engineering, Faculty of Engineering, NTNU, Norway
[b] Multiphase Flow, Department of Process Technology, SINTEF AS, Norway
[c] Statistics Group, Department of Mathematical Sciences, Faculty of Information Technology and Electrical Engineering, NTNU, Norway

ARTICLE INFO

Keywords:
Multiphase flow
Repeatability
Uncertainty
Pipe flow

ABSTRACT

A high degree of repeatability is most often an underlying assumption for research and development based on multiphase flow experiments. In this paper repeatability in multiphase flow experiments are studied through an experimental campaign with 28 replicates for 11 unique settings.

The experiments were conducted in a flow loop with multiple injections of oil, water and air. A high degree of repeatability was found, with relative replicate deviations in volume flow rates and pressure drops of 0.1% in magnitude. Further, several potential causes of replicate deviations were studied, and firmer control of temperature of the inflow fluids is proposed as a means to improve repeatability in volume flow rates and pressure.

We conclude that for practical use, the presented category of multiphase experiments sufficiently meets underlying repeatability assumptions.

1. Introduction

Multiphase flow in pipelines occur in many industrial applications and is especially important in the oil and gas industry (Ladva et al., 2000; Bratland, 2010; Osiptsov, 2017; Sun et al., 2018). Challenges of multiphase flow in pipes or channels include how the distribution of the phases in the cross section depends on the inflow rates, operational conditions, and thermodynamic state, leading to different multiphase flow regimes. With that in mind, models and simulators for multiphase flow in pipelines play important roles in hydrocarbon production, both during the field development and planning stage, and to ensure favorable flow conditions in the short- and long-term operation of pipelines (Gharaibah et al., 2015; Belt et al., 2011). Laboratory experiments support design and operation of field pipelines, either through tuning of simulator, calibration of experiments or otherwise representing the full-scale flow. Consequently, firm control and precision in the laboratory setting is essential for valid transfer to industry applications.

The development of models and simulators for multiphase flow in pipelines requires extensive high quality experimental data to cover a large span of the possible flow conditions may occur in field in practice (Shippen and Bailey, 2012). In multiphase experiments it is common not to repeat an experiment for a given setting, or to have only a few repeated experiments for some settings in an experimental campaign (Khor et al., 1997; Oddie et al., 2003; Babadagli et al., 2015; Leporini et al., 2019). This practice relies on an implicit assumption that performing the same experiment will give the same, or very similar, outcomes for the quantities of interest.

Repeatability is defined as measurement precision under conditions that include the same measurement procedure, same operators, same measuring system, same operating conditions and same location, and replicate measurements on the same or similar objects over a short period of time (BIPM et al., 2012). In this paper the aim is to study repeatability in a multiphase flow loop. To our knowledge there are no previous large studies of the implicit assumption of high degree of repeatability in multiphase pipe flow experiments.

We present highly unique experiments in a fixed multiphase pipe flow loop. A test matrix of 11 unique settings was replicated up to 28 times over the course of seventeen days. The experiments originally formed the foundation of a performance study of independent non-intrusive sensors where it was essential to provide identical volume flow rates of oil, water and air for each distinct setting repeatedly. The resulting data offered a rare opportunity to study repeatability of multiphase pipe flow experiments given instrumentation uncertainty, operational conditions and inflow conditions. In the described setup the mass flow rates where under automated regulation whereas pressure and temperature was not, apart from control of ambient temperature in the laboratory hall. Changes in fluid properties over time was also a factor to consider, especially for air and tap water.

* Corresponding author.
E-mail address: andreas.strand.so@gmail.com (A. Strand).

https://doi.org/10.1016/j.ijmultiphaseflow.2021.103886
Received 25 June 2021; Received in revised form 17 October 2021; Accepted 5 November 2021
Available online 27 November 2021

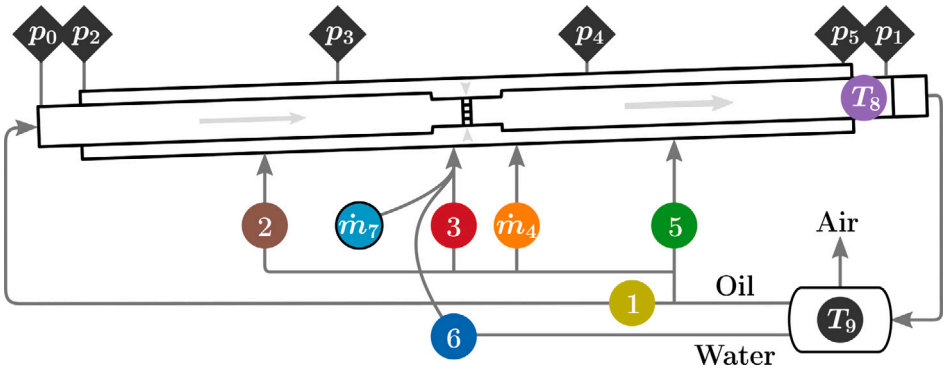

Fig. 1. The laboratory setup. A pipe of length 49 m encases another pipe. The pipes are coaxial with inclination of 2° upward. The diameters are amplified 20 times in the drawing compared to length. The main flow runs through the inner pipe. Secondary flow is injected into the annulus and enters the inner pipe through a perforation in the center. The flow components are oil (1, 2, 3, 4, 5), water (6) and air (7). During each cycle, the fluids mix and separate (9). The circles are meters for mass rate, density and/or temperature. The black diamonds are pressure meters, where p_2, p_3, p_4 and p_5 are annulus pressures. The pipe section at the outlet is partly transparent.

Table 1
Fluid system. Physical properties at 20°.

Fluid	Viscosity [Pa s]	Density [kg/m^3]
Exxsol D60	$1.39 \cdot 10^{-3}$	786
Tap water	$1.00 \cdot 10^{-3}$	1000
Air	$1.83 \cdot 10^{-5}$	1.204

Table 2
Measured variables with symbols, units and std. deviations of measurement errors.

Variable	Symbol	Unit	Standard deviation (σ)
Pressure	p	Pa/m	$p \cdot 0.09\,\%$
Air mass rate	$\dot{m}_7$	kg/s	$\dot{m}_7 \cdot 1.5\,\%$
Liquid mass rate	$\dot{m}$	kg/s	$\dot{m} \cdot 0.3\,\%$
Liquid density	ρ	kg/m^3	1 kg/m^3
Temperature	T	°C	0.21°C

The pipe inlet and outlet pressures along with volume flow rates were the primary quantities of interest. The main tasks were to (1) quantify repeatability of pressure measurements (2) quantify repeatability of volume flow rates (3) study possible causes of variation in pressure and volume flow rates through statistical modeling, using measurements of temperature, density, flow and pressure at multiple locations.

2. Experiments

The experiments were conducted at the SINTEF Multiphase Flow Laboratory. See Fig. 1 for a simplified drawing of the flow loop setup. The +2° inclined flow loop steel pipe test section consisted of

- a 49 m long fully welded inner pipe of inner/outer diameter 127.1/141.3 mm, with a 4.5 m long specially designed central inner pipe of inner/outer diameter 87.3/114.3 mm fitted to the main inner pipe by 127 mm long reducers; the central inner pipe had a perforated section consisting of 22 axial slits of dimensions 6.5 × 82.5 mm covering the pipe circumference to allow fluid flow into the base pipe from an external annular space;
- a 49 m long flanged outer pipe of inner/outer diameter 215.1/219.1 mm covering the inner pipe and defining an annular space between the coaxial inner and outer pipes; and
- 4 injections points at different axial locations along the test section for injection of fluids into the annular space. Upstream each injection point, a skid with regulation valves and flow meters controlled the mass inflow rates.

The box in Fig. 1 labeled T_9 represents a separation process, where fluids entered on the right-hand side. The upwards arrow represents air release, the line to 1 is oil and the line to 6 is water. The oil flow branched into the main flow 1 and the injection points 2, 3, 4 and 5. Air from 7 and water from 6 also entered at injection point 3. Exxsol D60 was used for the oil. The fluid properties at 20 °C are listed in Table 1.

2.1. Variables

The experiments were monitored by non-intrusive instruments, and their locations are shown Fig. 1. The black diamonds correspond to pressure meters, where p_0 is inlet, p_1 is outlet, and p_2, p_3, p_4 and p_5 are on the annulus. The remaining instruments are drawn as circles, numbered 1–9. Instruments $\dot{m}_4$ and $\dot{m}_7$ are mass rate meters. Locations 1, 2, 3, 5 and 6 each have meters for mass rate, density and temperature. Instrument T_8 is the outlet thermometer and T_9 is the separator thermometer.

All the measured variables with symbols and units are listed in Table 2. The measurements were associated with some error, with presumed standard deviations σ given in the last column of the table. In short, the standard deviations are quantified by the laboratory staff according to product specifications and experiments (Unander, 2021). The errors represent deviation from the physical value (JCGM, 1995). In addition, the physical values fluctuated slightly over a logging time of 5–10 min despite verification of a virtually steady state. Additional details on instrumentation are given in Appendix A.

2.2. Experimental design

The experiments originally supported a performance study of non-intrusive sensors from LYTT Ltd. However, the experimental design also conforms to a study of repeatability, and we reused the data for this purpose.

The mass rates at locations 1–7 were kept close to target levels by closed-loop control. Henceforth, one combination of target mass rates is called a setting. Eleven settings were used as shown in Table 3, each replicated between 23 and 28 times, according to the priorities in the original performance study. The column labeled 'Oil 1' gives the target main flow, which was alike for all settings. The remaining columns give the rates of injection into the annulus, where '–' corresponds to no injection at the given location. Additionally, setting 4 included 0.014 kg/m^3 sand and settings 5–7 included 0.057 kg/m^3 sand from annulus, but any impact from sand was not studied in this work.

On February 11, 2020 setting 1 was initialized. Steady-state was achieved after a couple of minutes, and then one set of measurements were made. Next, setting 2 was initialized, steady-state achieved and measurements made. The process continued according to numbering, and eventually setting 11 was measured. Thus far, one replicate of each setting was obtained. Again setting 1 was initialized, followed by

Table 3
Target mass rates of the experimental design. Eleven settings indexed in the first column. The number of replicates for each setting is given in column two. Columns 3–8 gives the mass rates in kg/s at each location. The value '–' corresponds to zero.

Setting	# replicates	Oil 1	Oil 2	Oil 3	Oil 4	Oil 5	Water (6)	Air (7)
1	28	4.318	–	–	–	–	–	–
2	28	4.318	0.720	0.720	–	0.720	–	–
3	26	4.318	0.720	2.159	–	0.720	–	–
4	26	4.318	0.720	0.720	–	0.720	–	–
5	27	4.318	0.720	0.720	–	0.720	–	–
6	26	4.318	0.720	0.720	–	0.720	–	–
7	28	4.318	0.720	0.720	0.720	0.720	–	–
8	26	4.318	–	–	–	–	2.746	–
9	23	4.318	–	1.079	–	–	1.373	–
10	28	4.318	–	–	–	–	1.373	–
11	28	4.318	0.720	0.720	0.720	0.720	–	0.02087

the same steps as above. Some of the iterations only included select settings, such that the number of replicates differ between settings. The process lasted until 28 replicates of setting 11 were obtained, at February 28, 2020.

In effect, the flow loop was reset between each run of the same setting. It is then correct to call each run a *replicate* rather than a repeat (Hamada et al., 2017). Yet, it is customary to use the term *repeatability* for the closeness of replicates, as explained in Section 3.

In terms of notation, let $i = 1, 2, \dots, 11$ be the setting index and let $j = 1, 2, \dots, n_i$ be the replicate index. Furthermore, index k refers to location as given in Fig. 1. Observations are written as x_{ijk} where x is pressure (p), mass rate ($\dot{m}$), density (ρ) or temperature (T).

2.3. Flow regimes

The 11 unique settings of the test matrix included 7 of single-phase oil, 3 of two-phase oil and water and 1 of two-phase oil and air. Depending primarily on inflow volumetric rates, pipe geometry and inclination, but also on the fluid properties and operational conditions, a wide range of flow regimes may arise, from stratified co-flow to gas–liquid slug flow, disperse flow and more. For gas–liquid flows an overview is given in (Mandhane et al., 1974; Açikgöz et al., 1992). For two phase oil–water flows additional flow regimes may arise, as presented by (Zavareh et al., 1988; Brauner and Maron, 1989). In order to assess flow-averaged characteristics of intermittent flow statistically, it is important that the intermittent variations of the flow are repeatable, meaning time periodic and with average values calculated over a long enough time for periodic structures to be taken into account. Hence, long transient phenomena such as surge waves and liquid accumulation are not permissible in such analyses. In our case the 3 two-phase oil–water experiment settings produced a stratified-wavy flow regime at the test section outlet, confirmed by visual inspection at the transparent pipe section. No evidence of liquid accumulation was found from investigation of the pressure sensor data in the remainder of the flow loop. For the two-phase oil–air flow setting, a slug flow regime was observed at the test section outlet, which was also evident from the time trace pressure signals. Importantly, the flow was strictly time periodic, and long transients were not observed.

3. Methodology

The International vocabulary of metrology (BIPM et al., 2012) defines several characteristics of replicated measurements, such as precision, accuracy and repeatability, which are quoted in Sections 3.1–3.3. In effect, these definitions agree with those of the International Organization for Standardization (ISO, 1994).

3.1. Measurement precision

Measurement precision is defined as "closeness of agreement between indications or measured quantity values obtained by replicate measurements on the same or similar objects under specified conditions". In our case, replicates refer to measurements $j = 1, 2, \dots, n_i$ of a fixed setting i and location k. The average over replicates is

$$\bar{x}_{ik} = \frac{1}{n_i} \sum_{j=1}^{n_i} x_{ijk}. \tag{1}$$

The measurement precision is in this work quantified as the relative deviation in each replicate from the sample mean, which is

$$\delta x_{ijk} = \frac{x_{ijk} - \bar{x}_{ik}}{\bar{x}_{ik}}. \tag{2}$$

3.2. Measurement accuracy

Measurement accuracy is defined as "closeness of agreement between a measured quantity value and a true quantity value of a measurand". The target mass rates $\dot{m}^0_{ik}$ given in Table 3 are *conventional quantity values*, which are canonical estimates for true quantity values (BIPM et al., 2012, Section 2.12). Measurement accuracy of mass rates is here defined by replacing the sample mean in (2) by m^0_{ik}, which gives

$$\delta_0 \dot{m}_{ijk} = \frac{\dot{m}_{ijk} - \dot{m}^0_{ik}}{\dot{m}^0_{ik}}. \tag{3}$$

3.3. Repeatability

Repeatability is measurement precision, see (2), under conditions that include "the same measurement procedure, same operators, same measuring system, same operating conditions and same location, and replicate measurements on the same or similar objects over a short period of time".

3.4. Liquid density model

Liquids expands with temperature. The rate of volume change due to temperature alone is

$$\frac{\mathrm{d}V}{\mathrm{d}T} = \alpha_k V, \tag{4}$$

where V is the volume of the fluid and α_k is the thermal expansion coefficient (Turcotte and Schubert, 2002). For our purpose (4) was represented in terms of densities and linearized about a temperature T^*. It was then necessary to assume α_k constant in temperature. The result was a linear regression model for density as a function of temperature,

$$d_k(T) = \hat{a}_k + \frac{\hat{b}_k}{1 + \alpha_k(T - T^*)}, \tag{5}$$

where $\hat{a}_k$ and $\hat{b}_k$ were coefficients obtained from ordinary least squares (Hastie et al., 2009) on observations T_{ijk} and ρ_{ijk} at settings K defined in Appendix B.3. Predictions from (5) are denoted $\hat{\rho}_{ijk} = d_k(T_{ijk})$. The residuals $\hat{\epsilon}_{ijk} = \rho_{ijk} - \hat{\rho}_{ijk}$ were the part of the density observations not modeled by temperature. Furthermore, the fraction of variance in density explained by temperature at location k was

$$r_k^2 = 1 - \frac{\sum_{i\in K}\sum_{j=1}^{n_i}\hat{\epsilon}_{ijk}^2}{\sum_{i\in K}\sum_{j=1}^{n_i}(\rho_{ijk} - \bar{\rho}_k)^2} = r^2(\rho_{ijk}, \hat{\rho}_{ijk}), \tag{6}$$

with r from (B.4) and $\bar{\rho}_k$ from (B.2). Conversely, $1 - r_k^2$ was the fraction of variance in density from other sources than temperature, according to the fitted regression model.

3.5. Air density model

The air was assumed dry with a specific gas constant of $R_{\text{air}} = 287.058\ \text{J/kg}\cdot\text{K}$. According to the ideal gas law, density is pressure p divided by temperature T and R_{air},

$$d_7(T, p) = \frac{p}{R_{\text{air}} T}. \tag{7}$$

The air density was not measured directly, only inferred from (7).

4. Results

4.1. Pressure measurements

Fig. 1 shows the placement of pressure meters. Fig. 2 gives all measurements for inlet pressure p_0 (crosses) and outlet pressure p_1 (circles) for all settings (frames) $i = 1, 2, \ldots, 11$. The vertical axes is pressure in kilopascal and the horizontal axes is time in days, from February 11 to 28 of year 2020. The horizontal axes are all identical. All vertical axes are of the same scale in order to provide visual comparisons of absolute replicate deviations.

Relative deviations in inlet pressure, outlet pressure and the pressure drop $p_1 - p_0$ was computed from (2) and is plotted in Fig. 3. The vertical axis is the number of observations that falls in each bin. The black curves are the distributions for each setting estimated by (B.1). The axes for the density curves are not included because the sole message is shape. The vertical dashed lines are ± 1 relative standard deviation in measurements, given in Table 2. Because inlet and outlet pressure had $\sigma = 0.09\%$, pressure drop had $\sigma = \sqrt{2}\cdot 0.09\% \approx 0.13\%$. The errors in instruments were treated as independent of each other. Fig. 4 gives the distributions of relative deviations in annulus pressures p_2, p_3, p_4 and p_5. All replicates of all settings are used for Figs. 3 and 4.

4.2. Deviations in volume flow rate

Volume flow rates dictates flow regime and is defined simply as $Q = \dot{m}/\rho$. Volume flow rate is proportional to mass flow rate, and inversely proportional to density. Note that Gaussian distributions for measurements of $\dot{m}$ and ρ implicates a Cauchy distribution for the volume flow rate (Pillai and Meng, 2016). The Cauchy distribution has no defined mean or variance. Consequently, it is impossible to directly translate the measurement error of mass flow rate and density to the volume flow rate.

The density was not measured at location 4, and ρ_1 was used as a proxy. The air density was not measured directly either, but inferred from (7). Air mixed with oil and was expected be at a temperature close to T_3 on annulus entry. Furthermore, air pressure was not measured at injection but instead approximated as p_4. In summary the reported injected air density was $d_7(T_{ij3}, p_{ij4})$.

The outlet volume rate was the sum of oil, water and air volume rates. Densities were not measured directly at the outlet, but both temperature T_8 and pressure p_1 were available. With densities from (5) and (7), the outlet volume rate was $Q_{ij8} = \sum_{k=1}^{7} \dot{m}_{ijk}/d_k(T_{ij8}, p_{ij1})$, where d_1 was used for all oil density models $d_1, d_2, \ldots, d_5$.

The relative deviations in replicate volume flow rates at locations 1–8 were computed from (2) and are presented in Fig. 5. Additionally, the outlet volume rates of oil, water and air were computed separately and the deviations in each are given in the bottom row of Fig. 5.

4.3. Deviations in mass flow rate

Recall that each experiment was run with certain target mass rates, which was automatically regulated. Relative deviations in mass flow rates computed from (3) are plotted in Fig. 6. For each location (frame), the histogram gives the distribution of relative errors over all settings and replicates. Naturally, only settings with flow at the given location were considered. An overview of the settings is given in Table 3.

4.4. Temperature series

The fluid temperatures were 15–19 °C for all experiments. The fluids expanded with temperature, and consequently the volume flow rate increased. Strict control of temperature was *not* imposed on the experiments, and fluctuations over time were expected. Fig. 7 gives all 294 measurements of temperatures T_1 (yellow crosses) and T_8 (purple circles). Location 1 and 8 are chosen as examples because they were relevant for all settings and relates to inlet and outlet. The horizontal axis represent time in days, with resolution of one minute. The trend each day was increasing temperature, on average 0.016 °C between subsequent measurements. However, 12 measurements (black) were clear exceptions to the trend, being at least 0.100 °C higher than the next measurement.

4.5. Density

Temperature was expected to be the main contributor to variation in density. The change in density was aptly modeled as locally linear in temperature as explained in Section 3.4. Linear models were fitted to oil ($k = 1$) and water ($k = 6$), where all measurements of temperature were within 1.5 °C of $T^* = 17.5$ °C. Thermal expansion coefficients were taken as $\alpha_1 = 7.64\cdot 10^{-4}\ ^\circ\text{C}^{-1}$ and $\alpha_6 = 2.14\cdot 10^{-4}\ ^\circ\text{C}^{-1}$. For clarity units are left out in the fitted models given by

$$d_1(T) = -662.16 + \frac{1450.30}{1 + 7.64\cdot 10^{-4}(T - 17.5)} \tag{8a}$$

and

$$d_6(T) = -99.56 + \frac{1095.88}{1 + 2.14\cdot 10^{-4}(T - 17.5)}. \tag{8b}$$

The fractions of explained variance were $r_1^2 = 99.3\%$ and $r_6^2 = 57.7\%$. The left panels of Fig. 8 show observations (circles) and the fitted models (black lines). The vertical axes are densities, and the horizontal axes are the temperature regressor (left) and the residuals (right). The residuals of the regressions are plotted against the fitted values and the vertical gray lines marks the value of zero.

5. Discussion

We have analyzed experiments in a flow loop with coaxial pipes and multiple injection points with the purpose of quantifying repeatability. Repeatability entails the ability to control the state of the flow loop, which is a desirable quality. The experiments were previously used to compare sensors, and the comparison benefitted from precision in volume rates and pressure across replicates. Precision in explanatory variables are also essential for tasks such as prediction.

The first results presented in Section 4 regarded repeatability of pressure measurements. As shown in Fig. 3, inlet pressure deviated

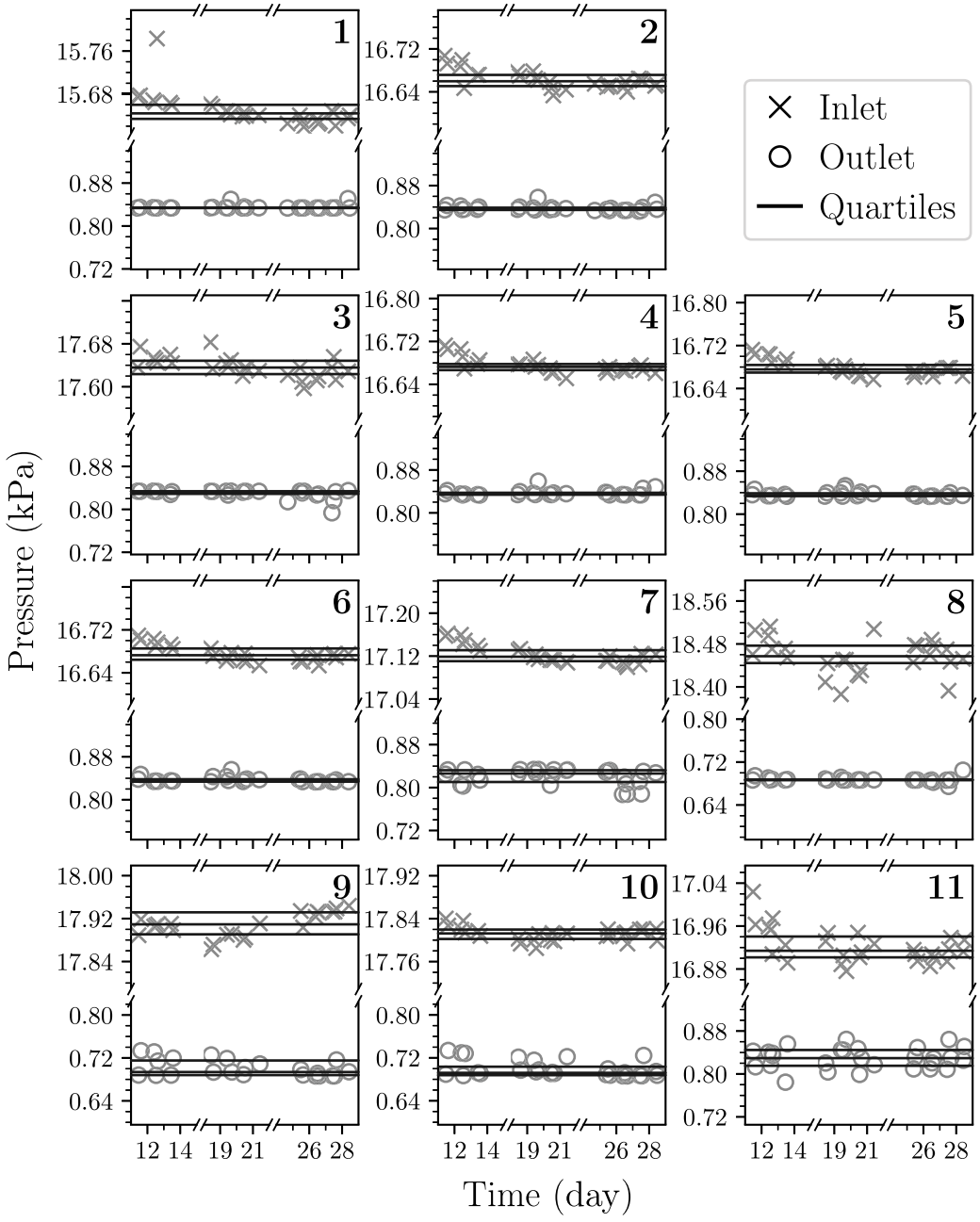

Fig. 2. Pressure measurements at inlet (crosses) and outlet (circles) for all settings 1–11 (frames). The vertical axes are pressure in kPa and the same scale is used in all frames. The horizontal axes are all identical and give time in days with a resolution of one minute. Quartiles of the measurements for each setting are drawn as horizontal lines.

less than 1% relative to the sample mean, and mainly less than 0.1%. The outlet pressure deviated less than 5%, and mainly less than 1%. The pressure drop $p_1 - p_0$ was of the same order of magnitude as the inlet pressure. All three distributions were bell-shaped and close to symmetric. The entropy of such distributions is large (Jaynes, 1957), which is appropriate for random errors.

The second panel of Fig. 3 gives the distribution for each setting as a black curve. Setting 11 had the largest deviations δp_{ij1}, followed by settings 9, 10 and 7. These were also among the most complex settings, as seen in Table 3. The large deviations in setting 11 were likely due to the introduction of air into the flow loop. Air flow in this study was more unstable than liquids due to compressibility effects, and air also affected the multiphasic fluid system in a complex manner which may have lead to a higher degree of variance compared to liquid-only flows. Fig. 4 gives the distributions of relative deviations in annulus pressures, which had higher variances than the inlet and outlet pressures. The positions of the annulus pressure meters are marked in Fig. 1. Clearly, the pressures in the upper part of the annulus were more variable, up to about 30% relative deviations. Setting 11 was least variable and is represented by the narrowest probability density curves in distributions for δp_{ij4} and δp_{ij5}. There was possibly a fluctuating mixture of air and liquid in the upper annulus for all settings except setting 11 where air constantly occupied the upper annulus.

It is instructive to study the causes of variation in pressure, starting with volume flow rates. Relative deviations are given in Fig. 5. The water rate was least variable, with most deviations smaller than 0.02% and the largest deviations at 0.06%. The deviations in oil inlet rates were about twice that. The deviations in injection rates Q_2 through Q_5 were less than 0.25% and mainly within 0.10%. The inlet air rates were more variable and deviated up to 0.80%. The behavior of the different fluids was reflected at the outlet. Both oil and water have similar deviations at outlet and inlet, while water deviates more at the

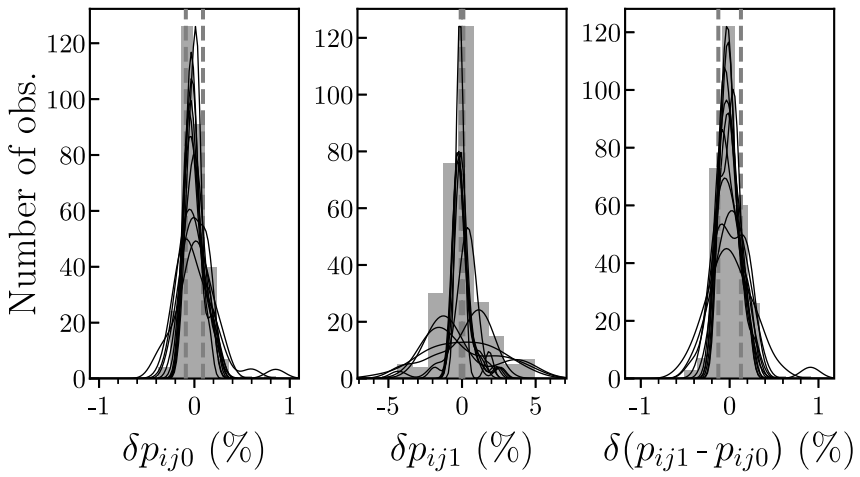

Fig. 3. Relative deviations in pressure from the setting averages, for inlet (left), outlet (middle) and difference (right). The frequency histogram gives the distribution of relative deviations. The black curves are fitted distributions for each setting (scaled to frame size). The dashed vertical lines represent the measurement standard deviations of the pressure meters.

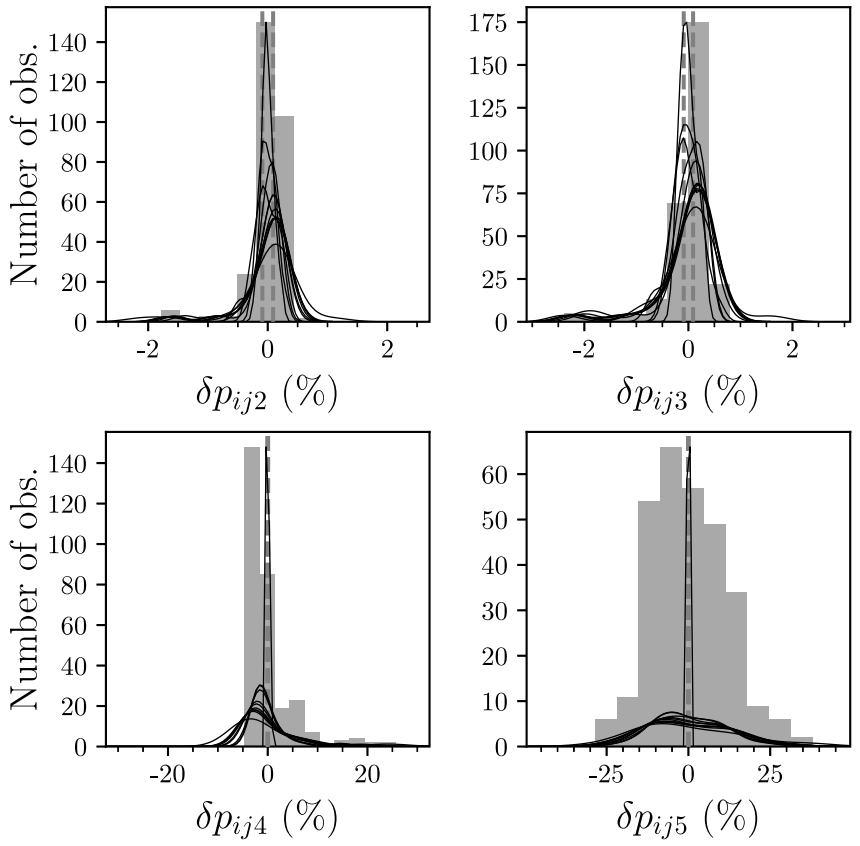

Fig. 4. Relative deviations in annulus pressure from the setting averages. For each location (frame), the histogram gives the distribution of relative deviations. The black curves are fitted distributions for each setting (scaled to frame size). The dashed vertical lines represent the measurement standard deviations of the pressure meters.

outlet, up to 5%. Volume flow rates impact pressure drop but the exact relation is complex for the flow loop considered. In the case of high flow rates, it is sometimes feasible to model pressure drop as a linear combination of the squared volume flow rates (Brown, 2000).

Volume flow rates were computed as mass flow rates divided by density. The mass rates deviations were well within one standard measurement errors of 0.3% and 1.5%. Of course, measurement errors also factored into the estimated relative deviations. In fact, the insight gained by comparing replicate deviations and measurement error is not clear. It is important to acknowledge that replicate deviations and measurement error are two distinct contributors to uncertainty about the physical values of the system variables. In our case, it seems that the prescribed measurement errors in the mass flow rates dominated the replicate deviations.

Fig. 7 shows that temperature increased over the course of a day, and surely the density decreased accordingly. The fitted linear models in Fig. 8 seemed appropriate and the residuals had no clear dependence on fitted densities. Moreover, temperature was estimated to explain 99.3% of the variance in oil density and 57.7% of the variation in water density. Most of the remaining variation in density is expected to be contamination of oil in water and vice versa. The separator did not

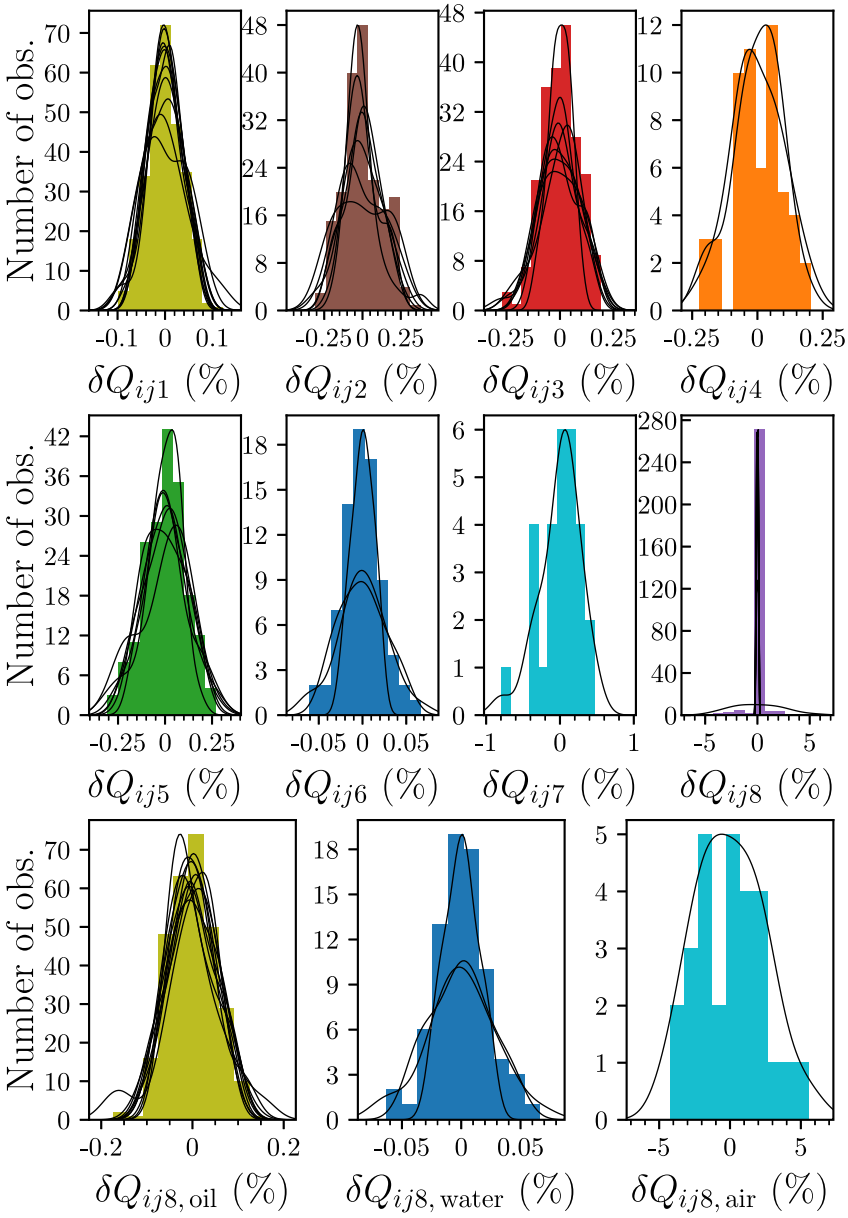

Fig. 5. Relative deviations in volume flow rate from the setting averages. For each location (frame), the frequency histogram gives the distribution of relative deviations. The black curves are fitted distributions for each setting (scaled to frame size).

perfectly separate oil and water, especially at high flow rates. Pressure would naturally also affect density to some extent.

Repeatability conditions is defined in Section 3.3 as a list of several requirements. Surely the replicates were conducted under the same measurement procedure, operators, measuring system and location, and describing similar objects. It is less obvious whether the operating conditions were sufficiently similar and whether the time span was short. It does not appear feasible to perform all experiments in significantly less time while also satisfying the remaining repeatability conditions. The time span would be reduced by considering fewer replicates, but at the cost of evidence. A shorter time span reduces the effect of confounders such as temperature. The temperature was not strictly controlled, yet no T_k spanned more than 2 °C. Each time a new setting was imposed on the flow loop, only a single replicate was produced, before changing to a different setting. The procedure was meticulous but denied bias from confounders. An even stronger insurance against confounders would be a fully random order of settings for each set of replicates.

With similar conditions across replicates, repeatability translates to measurement precision, which for this purpose is quantified as relative deviations in replicates given by (2). Distributions of relative deviations are provided in Figs. 3–6. Small deviations equal high repeatability which expresses the ability to impose specific conditions on the flow loop.

6. Conclusions

We have presented unique replicated experiments in a flow loop at the SINTEF Multiphase Flow Laboratory. Oil made up the main flow, but there were injections of oil, water and air through an annulus pipe surrounding the main test section. Eleven settings of the flow loop were run, ranging in complexity from only main flow to flow with several injections. Each setting was replicated up to 28 times. The conditions across replicates were compared and deemed sufficiently similar for a study of repeatability.

Inlet pressure, outlet pressure, pressure drop and volume flow rates were the quantities of interest. The relative deviations of all quantities

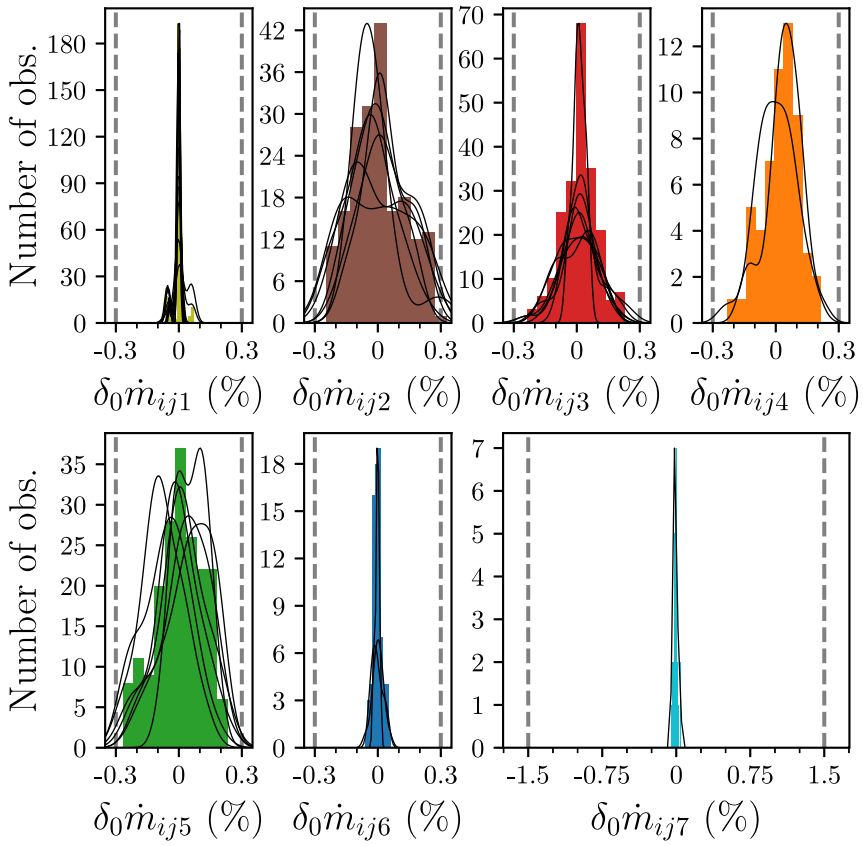

Fig. 6. Relative deviations from target mass flow rates. For each location (frame), the histogram gives the distribution of relative deviations. The black curves are fitted distributions for each setting (scaled to frame size). The dashed vertical lines represent the measurement standard deviations of the mass flow rate meters.

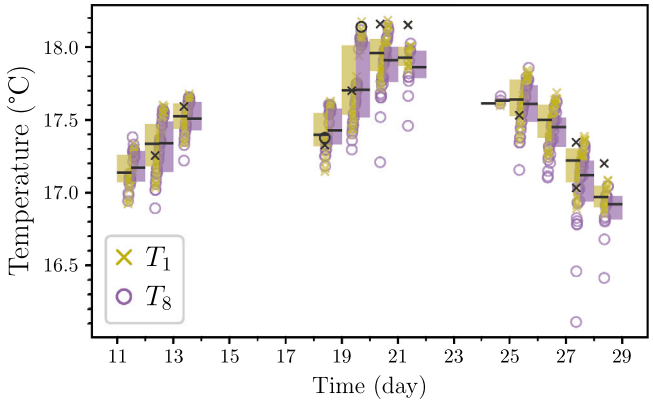

Fig. 7. Temperature (°C) for all experiments at location 1 (yellow crosses) and location 8 (purple circles). The horizontal axis gives the time of each measurement. Subsequent measurements are in most cases about ten minutes apart. Temperatures were mostly increasing throughout each day, and clear exceptions are drawn in black. Quartiles for each day and location are shown as boxes.

of interest were mainly much less than 1%. Effectively, the experiments were highly repeatable. In other words, the system for controlling the flow loop was capable of closely replicating select conditions.

Temperature explained 99.3% of the variance in oil density and 57.7% of the variance in water density. The density fluctuations directly changed the volume flow rates which in turn influenced the pressure drop. Temperature control was not a requirement in the original industrial test campaign from which the data was shared. Significantly higher repeatability is expected with strict control of the flow loop temperature.

The replicate deviations were small both in comparison to deviation across settings and measurement error. The high degree of repeatability observed is inevitably specific to the experimental setup. Still, it appears that satisfactory repeatability is achievable in multiphase experiments in flow loops akin to the presented setup.

CRediT authorship contribution statement

Andreas Strand: Conceptualization, Data curation, Formal analysis, Investigation, Methodology, Project administration, Resources, Software, Validation, Visualization, Writing – original draft, Writing – review & editing. **Christian Brekken:** Conceptualization, Data curation, Funding acquisition, Investigation, Methodology, Resources, Writing – original draft, Writing – review & editing. **Paul Roger Leinan:** Data curation, Investigation, Methodology, Resources, Writing – review & editing. **Ingelin Steinsland:** Conceptualization, Funding acquisition, Methodology, Supervision, Writing – review & editing. **Leif Rune Hellevik:** Conceptualization, Funding acquisition, Supervision, Writing – review & editing.

Declaration of competing interest

The authors declare that they have no known competing financial interests or personal relationships that could have appeared to influence the work reported in this paper.

Acknowledgments

LYTT Ltd. is acknowledged for sharing data for publication.

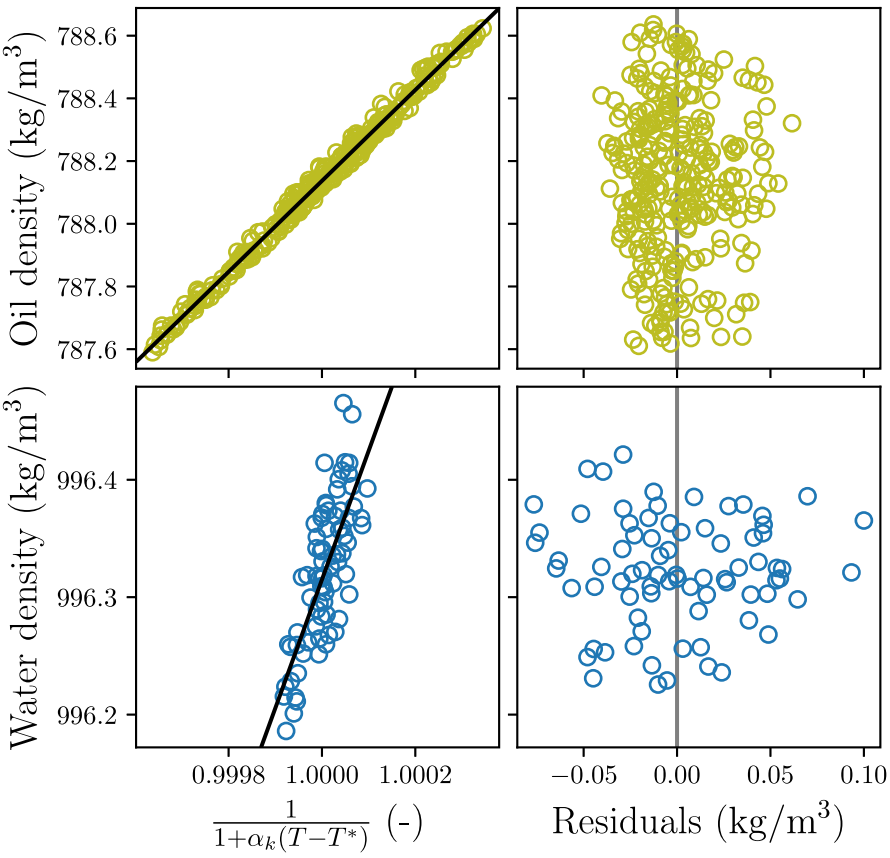

Fig. 8. Model for thermal expansion of oil (top) and water (bottom). Location 1 is used for oil. The density is given on the vertical axis for observations (circles) and fitted model (black line). The horizontal axis gives the transformed temperature (left) and regression residuals (right). Residuals are plotted against fitted values and the vertical gray line is where residuals are zero.

Appendix A. Instrumentation

The instruments used for measurements are listed in Table A.4. The measured variables are given in the first column. Note that some instruments measure multiple variables. The position of the instruments along the test section are given in the second column followed by a description in the last column.

Table A.4
List of measuring instruments with variables measured in the first column, position along the test section in meters in the second column and product description in the last column.

Variables	Position [m]	Instrument description
p_0	00.00	Fuji differential pressure transmitter
p_1	52.00	Fuji differential pressure transmitter
p_2	00.20	FUJI FCX-A/C II DP transmitter
p_3	16.30	Fuji differential pressure transmitter
p_4	32.40	Fuji pressure transmitter
p_5	48.40	Fuji pressure transmitter
$\dot{m}_1$, ρ_1	00.00	MicroMotion CMF200M elite series Coriolis meter
T_1	00.00	Inor Meso-HX temp transmitter with PT100 element, 3 mm edge and 1/2 inch tube clamp fitting
$\dot{m}_2$, ρ_2, T_2	11.60	Krohne Optimass 1400C S40
$\dot{m}_3$, ρ_3, T_3	23.60	Krohne Optimass 1400C S40
$\dot{m}_4$	27.60	Krohne Optimass 1400C S40
$\dot{m}_5$, ρ_5, T_5	37.60	Krohne Optimass 1400C S40
$\dot{m}_6$, ρ_6, T_6	23.60	Krohne Optimass 1400C S40
$\dot{m}_7$	23.60	Air flow meter EE771-CH1N025DKA1/RI6IMA P/N: S10757 S/N: 1702160000234C
T_8	52.00	PyroControl temperature transmitter rebuilt with PR5335D PT100
T_9	00.00	PyroControl temperature transmitter

Appendix B. Sample statistics

B.1. Kernel density estimation

The distribution of relative deviations in replicates δx_{ijk} for $j = 1, 2, \ldots, n_i$ was estimated as a Gaussian kernel with Scott's rule for bandwidth. Explicitly,

$$\hat{f}(z) = \frac{n_i^{5/4}}{\sqrt{2\pi}} \sum_{j=1}^{n_i} \exp\left(-\tfrac{1}{2} n_i^{2/5} (z - \delta x_{ijk})^2\right). \tag{B.1}$$

B.2. Mean and standard deviation

Let x_{ijk} be a measurement from an instrument, where x is a physical quantity, k is location, i is setting and j is replicate. Furthermore, let $K = \{i : \dot{m}_{ik}^0 > 0\}$ be the settings with flow at location k. The sample mean and unbiased sample standard deviation are

$$\bar{x}_k = \frac{1}{\sum_{i \in K} n_i} \sum_{i \in K} \sum_{j=1}^{n_i} x_{ijk} \tag{B.2}$$

and

$$\hat{\sigma}(x_k) = \sqrt{\frac{1}{\sum_{i \in K} n_i - 1} \sum_{i \in K} \sum_{j=1}^{n_i} \left(x_{ijk} - \bar{x}_k\right)^2}, \tag{B.3}$$

Table B.5
Means and standard deviations of pressure measurements in kPa. Values are given separately for each setting (rows 1–11) and overall (last row).

Set.	p_0		p_1		p_2		p_3		p_4		p_5	
	Mean	$\hat{\sigma}$	Mean	$\hat{\sigma}$	Mean	$\hat{\sigma}$	Mean	$\hat{\sigma}$	Mean	$\hat{\sigma}$	Mean	$\hat{\sigma}$
1	15.650	0.0307	0.835	0.00436	16.542	0.0963	11.152	0.0736	6.813	0.535	6.150	0.978
2	16.663	0.0179	0.838	0.00532	17.607	0.0726	12.236	0.0700	7.808	0.439	7.138	0.912
3	17.637	0.0197	0.830	0.00897	18.590	0.0659	13.220	0.0663	8.758	0.422	8.082	0.923
4	16.675	0.0149	0.837	0.00590	17.611	0.0732	12.241	0.0709	7.815	0.428	7.153	0.920
5	16.679	0.0146	0.837	0.00494	17.612	0.0708	12.241	0.0688	7.842	0.446	7.199	0.936
6	16.676	0.0153	0.837	0.00519	17.609	0.0687	12.237	0.0669	7.802	0.416	7.133	0.906
7	17.123	0.0177	0.820	0.01510	18.102	0.0621	12.727	0.0735	8.232	0.394	7.552	0.868
8	18.457	0.0331	0.687	0.00484	19.574	0.0376	14.183	0.0402	9.437	0.335	8.701	0.844
9	17.909	0.0228	0.701	0.01600	19.037	0.0346	13.642	0.0343	8.958	0.349	8.244	0.857
10	17.811	0.0125	0.699	0.01570	18.899	0.0185	13.526	0.0213	8.853	0.328	8.114	0.820
11	16.923	0.0322	0.829	0.02000	17.912	0.0244	12.527	0.0299	9.950	0.027	9.879	0.025
All	17.090	0.7480	0.797	0.06160	17.565	0.8190	12.700	0.8170	8.378	0.948	7.752	1.280

Table B.6
Means and standard deviations of density measurements in kg/m^3 at locations 1, 2, 3, 5 and 6. Values are given separately for each setting (rows 1–11) and overall (last row).

Setting	ρ_1		ρ_2		ρ_3		ρ_5		ρ_6	
	Mean	$\hat{\sigma}$	Mean	$\hat{\sigma}$	Mean	$\hat{\sigma}$	Mean	$\hat{\sigma}$	Mean	$\hat{\sigma}$
1	788.119	0.254								
2	788.181	0.249	782.763	0.310	783.238	0.273	781.888	0.609		
3	788.173	0.257	782.611	0.277	783.156	0.267	781.706	0.604		
4	788.166	0.252	782.657	0.265	783.197	0.261	781.920	0.598		
5	788.142	0.255	782.612	0.271	783.164	0.264	781.851	0.595		
6	788.137	0.252	782.600	0.259	783.155	0.257	781.848	0.567		
7	788.105	0.252	782.539	0.257	783.088	0.255	781.725	0.542		
8	788.087	0.254							996.356	0.0569
9	788.144	0.242			783.176	0.243			996.290	0.0528
10	788.141	0.242							996.317	0.0565
11	788.154	0.239	782.551	0.230	783.095	0.235	781.631	0.483		
All	788.141	0.247	782.619	0.273	783.158	0.257	781.795	0.572	996.212	0.203

Table B.7
Means and standard deviations of temperature measurements in °C at locations 1, 2, 3, 5, 6, 8 and 9. Values are given separately for each setting (rows 1–11) and overall (last row). Locations without flow are marked '–'. Air was only used at setting 11, with temperature T_7 of mean 18.96 °C and standard deviation 0.400 °C.

Set.	T_1		T_2		T_3		T_5		T_6		T_8		T_9	
	Mean	$\hat{\sigma}$	Mean	$\hat{\sigma}$	Mean	$\hat{\sigma}$	Mean	$\hat{\sigma}$	Mean	$\hat{\sigma}$	Mean	$\hat{\sigma}$	Mean	$\hat{\sigma}$
1	17.52	0.327									17.32	0.422	18.16	0.362
2	17.44	0.324	17.45	0.346	17.50	0.334	17.12	0.530			17.38	0.363	18.15	0.363
3	17.44	0.334	17.51	0.347	17.56	0.341	17.16	0.529			17.45	0.343	18.17	0.359
4	17.45	0.326	17.50	0.337	17.53	0.335	17.11	0.524			17.41	0.337	18.15	0.364
5	17.48	0.332	17.54	0.343	17.56	0.342	17.17	0.532			17.46	0.345	18.17	0.371
6	17.49	0.325	17.55	0.335	17.57	0.334	17.16	0.507			17.46	0.335	18.16	0.370
7	17.53	0.330	17.60	0.337	17.62	0.336	17.20	0.489			17.53	0.335	18.19	0.370
8	17.55	0.327							17.42	0.285	17.47	0.322	18.18	0.367
9	17.49	0.315			17.58	0.320			17.45	0.277	17.49	0.295	18.14	0.360
10	17.52	0.313							17.49	0.290	17.51	0.314	18.17	0.385
11	17.53	0.307	17.60	0.314	17.62	0.314	17.26	0.464			17.49	0.313	18.19	0.386
All	17.50	0.320	17.53	0.335	17.57	0.329	17.17	0.505	17.46	0.282	17.45	0.340	18.16	0.363

taken over all replicates j and settings $i \in K$. Tables B.5–B.7 lists the means and deviations of pressures, densities and temperatures for each setting separately and for all settings combined.

B.3. Correlation coefficient

Let x_{ijk} and y_{ijl} be measurements from two instruments, where x and y are physical quantities, k and l are locations, i is setting and j is replicate. The joint linear variation in x_{ijk} and y_{ijl} can be estimated by the sample Pearson correlation coefficient. Let $L = \{i : \dot{m}^0_{il} > 0\}$ be the settings with flow at location l, and let $M = K \cup L$. The correlation coefficient across all settings is

$$r(x_k, y_l) = \frac{\sum_{i\in M}\sum_{j=1}^{n_i}(x_{ijk} - \bar{x}_k)(y_{ijl} - \bar{y}_l)}{\sqrt{\sum_{i\in M}\sum_{j=1}^{n_i}(x_{ijk} - \bar{x}_k)^2}\sqrt{\sum_{i\in M}\sum_{j=1}^{n_i}(y_{ijl} - \bar{y}_l)^2}}, \tag{B.4}$$

with $\bar{x}_k$ and $\bar{y}_l$ from Eq. (B.2). The correlation coefficient between instruments succinctly pointed out physics of the system. The correlations between densities, temperatures and mass flow rates were estimated from (B.4) and illustrated in Fig. B.9. Each square in the grid, gives the correlation between the variables labeled on the axes. Values of larger magnitude than 0.6 is printed and the area of each square scales with magnitude.

The estimated correlation between the total mass flow rate $\dot{m}_1 + \dot{m}_2 + \cdots + \dot{m}_7$ and the pressure drop $p_1 - p_0$ was 0.54.

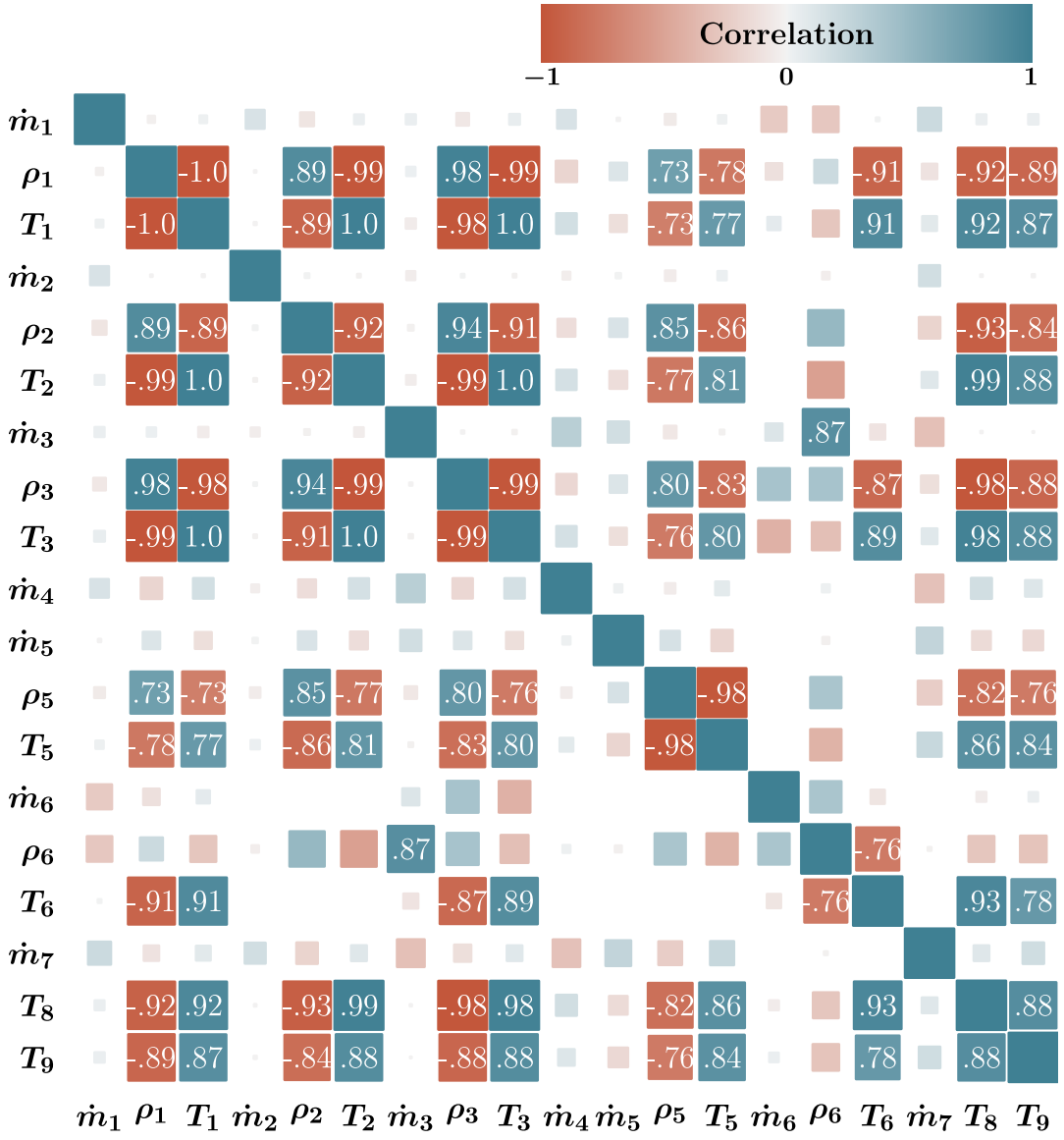

Fig. B.9. Correlation between variables. Each square gives the correlation between the variables on the axes. Correlation larger than 0.6 in magnitude are printed. The areas of the squares also represent magnitude.

References

Açikgöz, M., Franca, F., Lahey Jr., R., 1992. An experimental study of three-phase flow regimes. Int. J. Multiph. Flow. 18 (3), 327–336.

Babadagli, T., Ren, X., Develi, K., 2015. Effects of fractal surface roughness and lithology on single and multiphase flow in a single fracture: An experimental investigation. Int. J. Multiph. Flow. 68, 40–58.

Belt, R., Duret, E., Larrey, D., Djoric, B., Kalali, S., 2011. Comparison of commercial multiphase flow simulators with experimental and field databases. In: International Conference on Multiphase Production Technology. All Days, URL https://onepetro.org/BHRICMPT/proceedings-pdf/BHR11/All-BHR11/BHR-2011-I2/1663541/bhr-2011-i2.pdf, BHR-2011-I2.

BIPM, I., IFCC, I., IUPAC, I., ISO, O., 2012. International Vocabulary of Metrology–Basic and general concepts and associated terms (VIM), 3rd edn JCGM, p. 200, URL https://www.bipm.org/utils/common/documents/jcgm/JCGM_200_2012.pdf, Accessed on April 3, 2021.

Bratland, O., 2010. Pipe flow 2, multiphase flow assurance, electronic book. URL http://drbratland.com/PipeFlow2/.

Brauner, N., Maron, D.M., 1989. Two-phase liquid-liquid stratified flow. Physiochem. Hydrodyn. 11, 487–506.

Brown, G., 2000. The Darcy-weisbach equation. Okla. State Univ.–Stillwater.

Gharaibah, E., Read, A., Scheuerer, G., et al., 2015. Overview of CFD multiphase flow simulation tools for subsea oil and gas system design, optimization and operation. In: OTC Brasil. Offshore Technology Conference, 26326.

Hamada, M.S., Steiner, S.H., MacKay, R.J., Reese, C.S., 2017. Planning and analyzing experiments with models that distinguish between replicates and repeats. Qual. Reliab. Eng. Int. 33 (3), 657–668.

Hastie, T., Tibshirani, R., Friedman, J., 2009. The Elements of Statistical Learning: Data Mining, Inference, and Prediction. Springer Science & Business Media.

ISO, 1994. Accuracy (Trueness and Precision) of Measurement Methods and Results – Part 1: General Principles and Definitions, Vol. 1994. International Organization for Standardization, Geneva, CH.

Jaynes, E.T., 1957. Information theory and statistical mechanics. Phys. Rev. 106 (4), 620.

JCGM, 1995. Guide to the expression of uncertainty in measurement. URL https://www.bipm.org/utils/common/documents/jcgm/JCGM_100_2008_E.pdf, Accessed on March 17, 2021.

Khor, S., Mendes-Tatsis, M., Hewitt, G., 1997. One-dimensional modelling of phase holdups in three-phase stratified flow. Int. J. Multiph. Flow. 23 (5), 885–897.

Ladva, H., Tardy, P., Howard, P., Dussan V, E., et al., 2000. Multiphase flow and drilling fluid filtrate effects on the onset of production. In: SPE International Symposium on Formation Damage Control. Society of Petroleum Engineers, 58795.

Leporini, M., Marchetti, B., Corvaro, F., Di Giovine, G., Polonara, F., Terenzi, A., 2019. Sand transport in multiphase flow mixtures in a horizontal pipeline: An experimental investigation. Petroleum 5 (2), 161–170.

Mandhane, J., Gregory, G., Aziz, K., 1974. A flow pattern map for gas—liquid flow in horizontal pipes. Int. J. Multiph. Flow. 1 (4), 537–553.
Oddie, G., Shi, H., Durlofsky, L., Aziz, K., Pfeffer, B., Holmes, J., 2003. Experimental study of two and three phase flows in large diameter inclined pipes. Int. J. Multiph. Flow. 29 (4), 527–558.
Osiptsov, A.A., 2017. Fluid mechanics of hydraulic fracturing: A review. J. Pet. Sci. Eng. 156, 513–535.
Pillai, N.S., Meng, X.-L., 2016. An unexpected encounter with Cauchy and Lévy. Ann. Statist. 44 (5), 2089–2097. http://dx.doi.org/10.1214/15-AOS1407, URL https://doi.org/10.1214/15-AOS1407.
Shippen, M., Bailey, W.J., 2012. Steady-state multiphase flow – past, present, and future, with a perspective on flow assurance. Energy Fuels 26 (7), 4145–4157.
Sun, B., Guo, Y., Sun, W., Gao, Y., Li, H., Wang, Z., Zhang, H., 2018. Multiphase flow behavior for acid-gas mixture and drilling fluid flow in vertical wellbore. J. Pet. Sci. Eng. 165, 388–396.
Turcotte, D.L., Schubert, G., 2002. Geodynamics. Cambridge University Press.
Unander, T., 2021. Uncertainty Quantification in Multiphase Pipe Flow Experiments. Tech. Rep. 00102, SINTEF, ISBN 978-82-14-06488-9.
Zavareh, F., Hill, A., Podio, A., 1988. Flow regimes in vertical and inclined oil/water flow in pipes. In: SPE Annual Technical Conference and Exhibition. OnePetro, 18215.